H2SO4 and Organosulfur Compounds in Laboratory Analogue Aerosols of Warm High-metallicity Exoplanet Atmospheres

Véronique Vuitton, Sarah E Moran, Chao He, Cédric Wolters, Laurene Flandinet, François-Regis Orthous-Daunay, Julianne I Moses, Jeff A Valenti, Nikole Lewis, Sarah Hörst

The Planetary Science Journal, 2:2 (11pp), 2021 February https://doi.org/10.3847/PSJ/abc558

H_2SO_4 and Organosulfur Compounds in Laboratory Analogue Aerosols of Warm High-metallicity Exoplanet Atmospheres

Véronique Vuitton[1], Sarah E. Moran[2], Chao He[2], Cédric Wolters[1], Laurène Flandinet[1], Francois-Régis Orthous-Daunay[1], Julianne I. Moses[3], Jeff A. Valenti[4], Nikole K. Lewis[5], and Sarah M. Hörst[2]
[1] Univ. Grenoble Alpes, CNRS, CNES, IPAG, 38000 Grenoble, France; veronique.vuitton@univ-grenoble-alpes.fr
[2] Department of Earth and Planetary Sciences, Johns Hopkins University, Baltimore, MD 21218, USA
[3] Space Science Institute, Boulder, CO, USA
[4] Space Telescope Science Institute, Baltimore, MD, USA
[5] Department of Astronomy and Carl Sagan Institute, Cornell University, Ithaca, NY, USA
Received 2020 September 10; revised 2020 October 14; accepted 2020 October 26; published 2021 January 22

Abstract

Recent transit spectra suggest organic aerosol formation in the atmosphere of sub-Neptunes. Sulfur gases are expected to be present in warm exoplanet atmospheres with high metallicity. Many aspects of the sulfur fixation process by photochemistry in planetary atmospheres are not fully understood. In this work, tholins produced in a CO_2-rich atmosphere simulation experiment with H_2S were analyzed with very high-resolution mass spectrometry (HRMS) that allows for searching specific molecules in addition to providing some insight on the mixture complexity. To our knowledge, this is the first experimental investigation of sulfur-bearing organic aerosol formation from irradiation of H_2S at temperatures relevant to warm exoplanets. The analysis of the mass spectra shows that the soluble organic fraction of the solid particles contains over 2500 organosulfur (CHS/CHOS/CHNS/CHNOS) molecular formulas (73% of all assigned signals) within a broad mass range (from 50 to 400 u, atomic mass unit). In particular, 14 sulfuric acid derivatives were detected and 13 unique molecular formulae that could correspond to amino acid derivatives were identified. This high molecular diversity indicates a rich and active sulfur chemistry triggered by irradiation of H_2S. The average elemental composition (wt%) of the soluble fraction of the particles is 40%C, 30%O, 21%S, 6%H, and 3%N, making the sulfur abundance a factor of ∼14 larger than in the initial gas composition. Our analysis of experimental simulations shows that organosulfur species are likely an important component of the haze in exoplanet atmospheres.

Key words: Molecule formation – Exoplanet atmospheric composition – Laboratory astrophysics – Mass spectrometry

1. Introduction

Transit spectra have suggested that condensate clouds and/or photochemical haze are present in the atmospheres of several super-Earths and mini-Neptunes (GJ3470b, GJ1214b, Kepler 51b, and GJ436b) (Benneke et al. 2019; Kreidberg et al. 2014; Libby-Roberts et al. 2020; Lothringer et al. 2018). However, little is known about the composition and optical properties of these particles. Organic aerosols affect chemistry, radiation flux, and dynamics: they can provide organic material to the surface and/or change its temperature and therefore have an impact on the habitability of the planet (Marley et al. 2013). Haze absorption features could be detected by the James Webb Space Telescope, but could also hide the spectral signatures of gaseous constituents, preventing atmospheric characterization (e.g., Arney et al. 2017).

It is extremely challenging to theoretically simulate the complex chemical processes for haze formation in planetary atmospheres due to a lack of chemical kinetics information under relevant conditions. Another way to study hazes is to synthesize analogues in the laboratory, called tholins, and to analyze them with state-of-the-art analytical instruments. Experimental data on the physical structure, optical properties, and chemical composition of organic aerosols have led to tremendous progress in our understanding of their formation processes on Titan and the early Earth (Cable et al. 2012). However, experimental work to characterize the properties of photochemical hazes formed in atmospheres exotic to our solar system is still in its infancy.

We have performed a series of laboratory atmosphere simulation experiments dedicated to the characterization of haze analogues synthesized under a broad range of atmospheric parameters relevant to super-Earths and mini-Neptunes. Nine different gas mixtures dominated by either H_2, H_2O, or CO_2 and with fractions of CH_4, CO, NH_3, and N_2 were exposed to a plasma or ultraviolet (UV) photons at temperatures ranging from 300 to 600 K. The gas compositions correspond to the most likely "primordial" atmospheric compositions ($10^2\times$, $10^3\times$, $10^4\times$ solar metallicity, 300–600 K) as suggested by thermochemical-equilibrium calculations (Moses et al. 2013). We showed that the production rates and physical properties of the particles vary widely depending on the gas mixture composition (Hörst et al. 2018; He et al. 2018a, 2018b). Many complex molecular species with general chemical formulas $C_cH_hN_nO_o$ were detected, possibly including some of prebiotic interest (Moran et al. 2020).

Sulfur and phosphorus are the next most abundant chemically reactive volatile elements after hydrogen, carbon, nitrogen, and oxygen, in a solar system composition gas. SO_2 is a common volcanic gas on Earth, Venus, and Io, the innermost moon of Jupiter, and its photochemical products significantly shape the spectra of these bodies; the most striking example is

the high planetary albedo of Venus's atmosphere due to thick sulfuric acid (H_2SO_4) clouds (Titov et al. 2018). H_2S is expected to be the dominant reservoir of sulfur in warm reduced exoplanet atmospheres under equilibrium chemistry (Gao et al. 2017). However, experimental investigations for sulfur-bearing organics have been restricted to studies using SO_2 (Farquhar et al. 2001; DeWitt et al. 2009) or H_2S in CH_4/N_2 (Reed et al. 2020). To our knowledge, no photochemical investigation of sulfur-bearing organic aerosol formation from irradiation of H_2S in CO_2 dominated atmospheres has been conducted and the role of S atoms in the subsequent complex chemistry is largely unknown.

We investigated the impact of H_2S in high metallicity (10,000x solar) exoplanet atmospheres by studying the gas-phase composition and the particle production rate and size (He et al. 2020a). However, sulfur photochemistry is poorly understood, and it is not clear how much and by what mechanism sulfur is incorporated in organic aerosols. Our objective in this contribution is now to evaluate the molecular diversity of the particles and for this purpose, we analyze the soluble fraction using very high-resolution mass spectrometry (HRMS). Sulfur is an essential biotic element. Understanding the formation chemistry and the resulting chemical structure of possible S-bearing organic aerosols in warm CO_2-rich atmospheres will help constrain the atmospheric contribution in abiotic sulfur fixation processes relevant to the origin and evolution of early life.

2. Experiments

2.1. Sample Synthesis and Preparation

Organic particles were synthesized at Johns Hopkins University, in the Planetary HAZE (PHAZER) simulation chamber for planetary atmospheres (Figure 1 in He et al. 2020a). The initial gas mixture for our experiments is 47% CO_2, 23% CO, 11% N_2, 8.7% H_2, 4.4% He, 4.3% H_2O, and 1.6% H_2S, calculated from a chemical equilibrium model for $10^4\times$ solar metallicity at 800 K and 1 mbar (Moses et al. 2013), where we retained only the gas-phase species with mixing ratios greater than 1%, and then renormalized the remaining gases to 100%. It is heated to 800 K by flowing through a heating coil and exposed to an AC glow discharge having an estimated energy density of 170 W m^{-2}. The pressure in the reaction chamber is a few mbar and the flow rate is maintained at 10 sccm (standard cubic centimeters per minute). The experiment runs continuously for 72 h, ultimately leading to the formation of a solid product. We ran a reference experiment with the same gas mixture but without plasma. The AFM images showed that no particles were produced in the reference experiment (He et al. 2020b). More details about the haze production setup and the experimental procedure can be found in previous studies (He et al. 2018a, 2018b, 2019, 2020a, 2020b; Hörst et al. 2018; Moran et al. 2020).

2.0 mg of tholin powder was sequentially dissolved in 1.30 mL of polar and apolar solvents, vortexed for 1 hour and centrifuged at 10,000 rpm for 10 min (Moran et al. 2020). The considerable difference of the resulting Orbitrap mass spectra denotes distinct solvent extraction efficiencies. The 1:1 CH_3OH: CH_2Cl_2 solution (CH_3OH, Lichrosolv Merck, UHPLC-MS grade $\geqslant$99.9%; CH_2Cl_2, Uvasol Merck, GC purity $\geqslant$99.9%) gives the best results with respect to yield as well as to composition and these results only are presented here. Nevertheless, a visible fraction of the solid remained insoluble. Previous work on CHON-containing tholins has shown that insoluble molecules are less hydrogenated than the soluble molecules and extend to heavier molecular weights (Maillard et al. 2018). Nevertheless, the soluble fraction has an elemental abundance similar to the bulk (Moran et al. 2020).

2.2. Mass Spectrometry Analysis

The analysis of the tholins was performed with the Orbitrap mass spectrometer located at Institut de Planétologie et d'Astrophysique de Grenoble (LTQ-Orbitrap XL™, Thermo Fischer Scientific). This instrument has been widely used by our group for in-depth molecular characterization of extra-terrestrial organic matter (Bonnet et al. 2013; Danger et al. 2013; Gautier et al. 2020; Hörst et al. 2012; Moran et al. 2020; Somogyi et al. 2016; Vuitton et al. 2010). Data acquisition was performed using the LTQ Tune Plus software provided by the manufacturer. A time-domain transient is Fourier-transformed into a frequency-domain spectrum, which is converted to a mass spectrum. The mass resolving power ($m/\Delta m_{50\%}$, in which $\Delta m_{50\%}$ is the mass spectral peak FWHM peak height) is >100,000 up to $m/z = 400$ with a mass accuracy of <5 ppm. The instrument is externally calibrated daily by using the manufacturer's Calmix calibration solution (caffeine, MRFA peptide, Ultramark 1621 in the positive ionization mode and sodium dodecyl sulfate, sodium taurocholate, Ultramark 1621 in the negative ionization mode) in the mass range $m/z =$ 200–2000.

An electrospray ionization source (Ion Max™ ESI, Thermo Fischer Scientific) was used in both positive and negative ionization modes. The ESI ionization technique does not fragment the molecular species. Indeed, the species are only protonated and detected as $[M+nH]^{n+}$ or $[M-nH]^{n-}$ when operating in positive or negative ionization mode, respectively. As a consequence, hydrocarbons and sulfur-containing compounds such as thiophenes and S_n, which are not sufficiently acidic or basic, are not efficiently ionized by ESI. The solutions were directly infused into the ionization source at a flow rate of 3 μL min^{-1}. Full scan mode mass spectra were acquired for a total mass range of $m/z = 50$–450 divided into two subranges of $m/z = 50$–300 and $m/z = 150$–450, using an AGC setting of 5×10^5 ions. For each mass spectrum, four scans of 128 microscans were accumulated as microscans enhance signal quality by lowering noise and reducing artifacts (Wolters et al. 2020). A source voltage of 3.5 kV was used in positive ionization mode and 3.8 kV in negative ionization mode. The sheath, auxiliary, and sweep gas flow rates were set at 5, 0, and 0 (arb. unit), respectively. The source position was (B;1) in positive ionization mode and (C;1.5) in negative ionization mode. The capillary voltage and temperature were maintained at 34 V and 275 °C, respectively. The tube lens voltage was kept at 50 V for the lower mass range and 70 V for the higher mass range (−50/−70 V in negative mode). Blanks were measured immediately prior to the tholins analysis to be able to differentiate the soluble organic matter of the tholin sample from contaminations that could arise in preparing the samples. They account for the solvent as prepared on the petri dishes and in the vials.

Preliminary visualization was performed with the XCalibur software provided by the manufacturer. A custom software developed at IPAG was then used to extract data from .raw files. The extraction is based on an IGOR Pro (WaveMetrics,

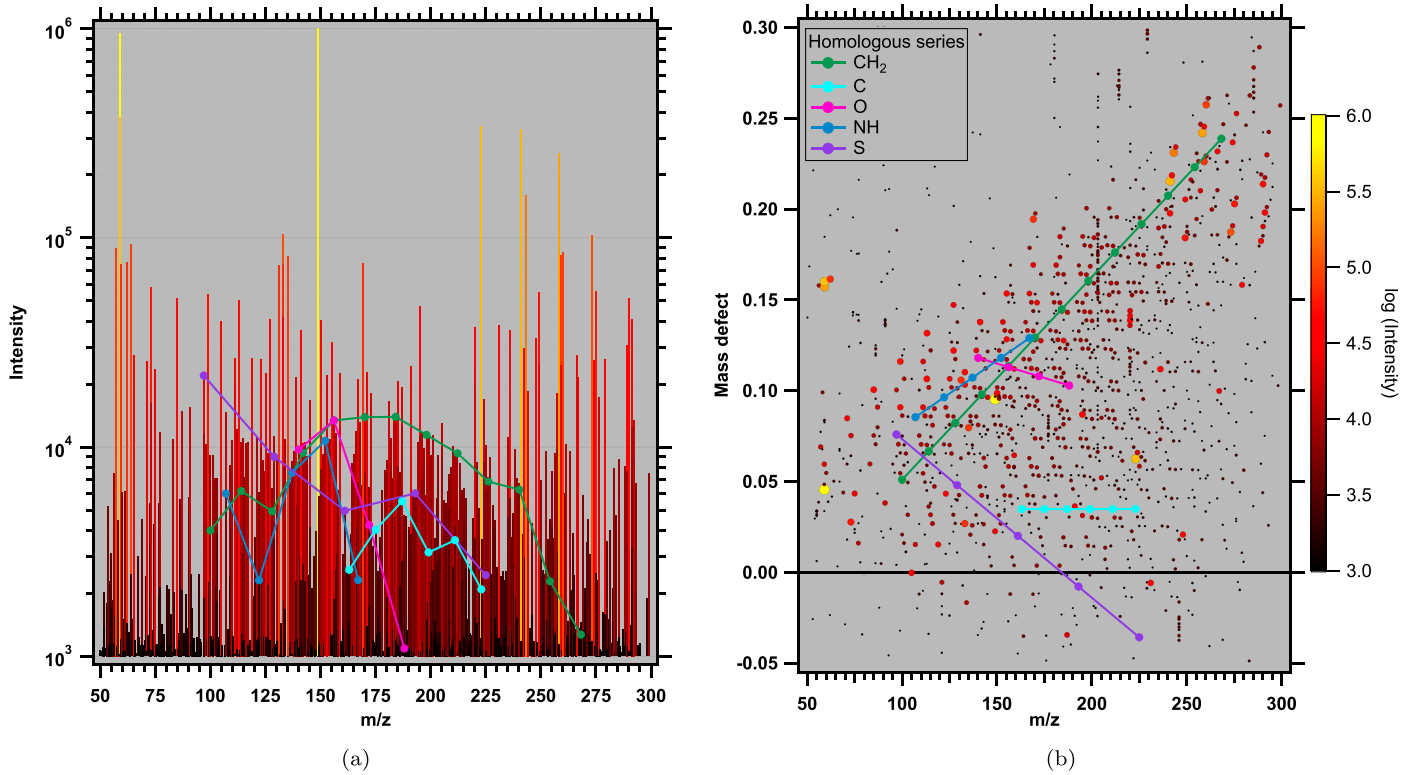

Figure 1. Mass spectrum from $m/z = 50$ to 300 of tholins ($10^4\times$ metallicity, 800 K) in positive ionization mode. (a) Classical representation of the intensity versus mass-to-charge ratio (m/z), in logarithmic scale. (b) Mass defect versus m/z. Alignments of points are due to recurrent stoichiometric differences such as CH_2, C, O, NH, and S.

USA) routine that uses Windows open libraries to open and read directly the data inside the .raw files. After data extraction, each scan is summed to produce a single resulting mass spectrum. Then, this mass spectrum is loaded into "Attributor", an in-house software tool developed to treat and attribute HRMS data. Each spectrum is converted from peak profile to centroids (exact m/z values), and molecular formulas are assigned by solving the Diophantine equation where the constant coefficients are stoichiometric groups (CH_2, C, NH, O, and S; Orthous-Daunay et al. 2020), considering that only singly charged (de-)protonated ions are formed. Some ^{13}C and ^{34}S stoichiometric formulas are detected but only the corresponding ^{12}C and ^{32}S isotopologs are considered further in this study.

2.3. Data Treatment and Representation

At our Orbitrap mass resolving power ($m/\Delta m_{50\%} \approx 100{,}000$), it is possible to resolve close mass doublets (notably, elemental compositions differing by C_3 versus SH_4, 0.003 4 Da) up to $m/z \sim 300$. The mass accuracy (<5 ppm) also allows for assignment of a unique elemental composition, $C_cH_hN_nO_oS_s$, to singly charged ions up to $m/z \sim 300$. At higher mass, assignment based on mass measurement accuracy alone is no longer unique within experimental mass measurement error. The methylene (–CH_2–) group is the most relevant nominal building block of organic chemistry, even if of nonterrestrial provenance (Schmitt-Kopplin et al. 2010). To extend unique elemental composition assignment to higher mass, we start from unique mass assignment at low mass and identify the other members of an alkylation series (namely, compounds with a given number of N, O, and S atoms, and different numbers of CH_2 groups), so that unique elemental compositions may be assigned to ions over the entire mass range analyzed ($m/z = 50$–450). To allow for recognition and graphical resolution of various homologous series, we introduced the "MDvM" plot, namely, a plot of mass defect (difference between exact mass and nominal mass) versus nominal mass, in which nominal mass is the mass rounded to the nearest integer value (Danger et al. 2013). The MDvM plot highlights nonrandomness in the mass distribution by producing rows of data where compounds are separated by repetitive molecular groups. In the MDvM diagram shown in Figure 1, specific trend lines corresponding to the repetition of a number of CH_2, C, O, NH, and S groups are highlighted, reflecting a pure chemosynthetic process (Orthous-Daunay et al. 2019).

The mass spectra were then recalibrated with respect to identified alkylation series. In the negative ionization mode, naturally occurring fatty acids were readily recognized and calibrated with accuracies <1.0 ppm, and subsequently removed from the data set. To obtain the molecular formula, one proton is either added (negative mode) or subtracted (positive mode) from the molecular ion formula. A direct comparison can then take place between data sets recovered from positive and negative ionization modes and all analyses were performed on the resulting data set. More details on the acquisition of Orbitrap data and the assignment of molecular formulas are given in previous studies (Danger et al. 2016; Fresneau et al. 2017; Jovanović et al. 2020).

Though Orbitrap MS data can be treated by "MDvM" analysis to identify molecules that differ by the exact mass of CH_2 or other groups, they provide no information about the rest of the molecule. On the other hand, one piece of bulk structural information that can be calculated from HRMS data is unsaturation. In the determination of chemical structures from

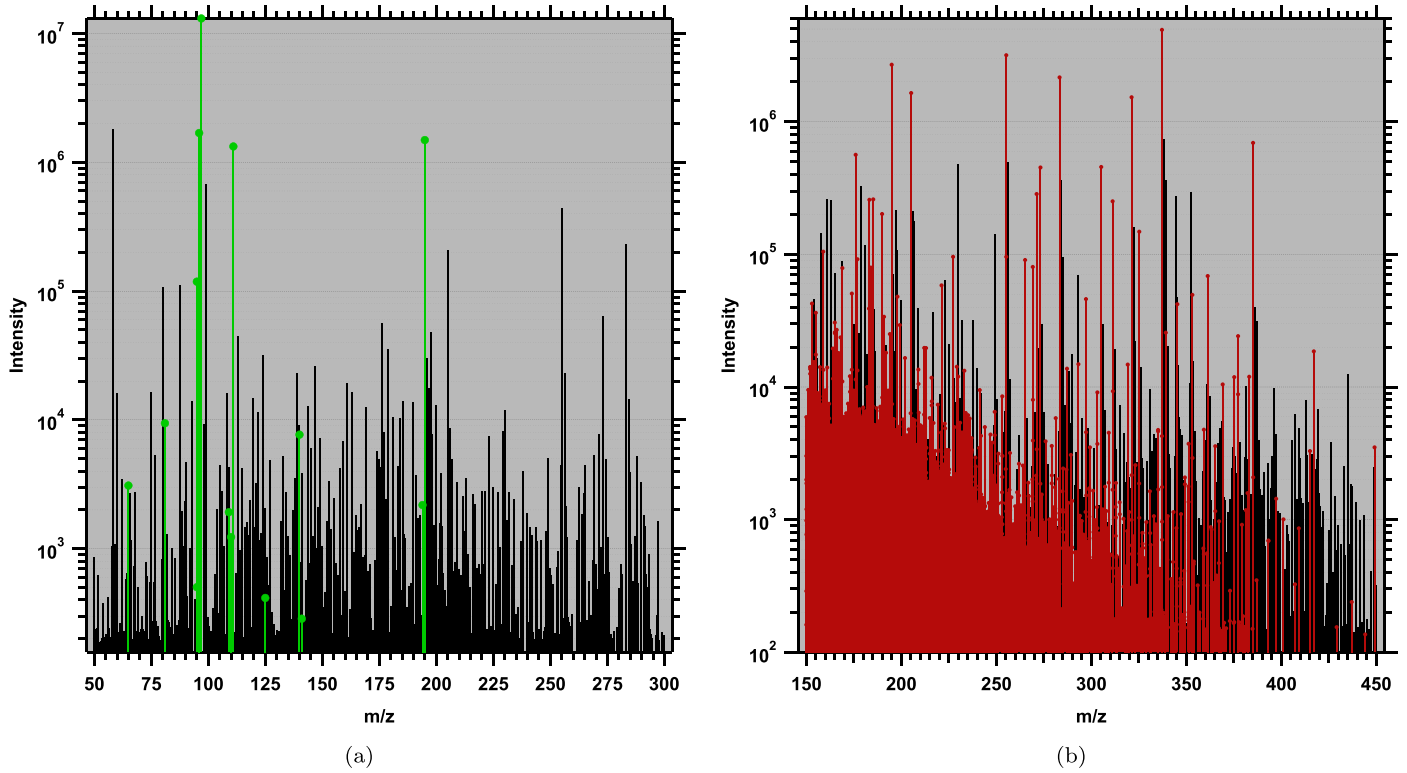

Figure 2. Mass spectra of tholins in negative ionization mode. (a) *m/z* = 50 to 300. The most intense peaks, highlighted in green, are attributed to sulfuric acid and some of its derivatives (Table 1). (b) *m/z* = 150 to 450. Over 2700 organosulfur peaks (CHNOS), highlighted in red, are distributed over this mass range. Most signals above *m/z* 400 cannot be attributed to CHONS species and correspond to random noise.

molecular formulas $C_cH_hN_nO_oS_s$, it is often useful to calculate the number of double bond equivalents (DBE), defined as the number of rings plus double bonds in a neutral molecule:

$$\mathrm{DBE} = 1 + \frac{1}{2}\left(\sum_i n_i(\nu_i - 2)\right), \tag{1}$$

with n_i the number, and ν_i the formal valence of the element i.

The DBE calculation is strictly accurate for most of the organic molecules containing only C, H, N, and O. However, if sulfur is present in a molecule, its formal valence depends on its form and has, for example, different values if sulfur occurs in the molecule as a sulfide ($\nu = 2$), a sulfoxyde ($\nu = 4$), or a sulfone ($\nu = 6$). As we do not know the structure(s) associated to our univocal molecular formulae, we consider the extreme cases where $\nu_S = 2$ and $\nu_S = 6$, giving the following general formulae:

$$\mathrm{DBE}(\nu_S = 2) = c - \frac{h}{2} + \frac{n}{2} + 1 \tag{2a}$$

$$\mathrm{DBE}(\nu_S = 6) = c - \frac{h}{2} + \frac{n}{2} + 2s + 1. \tag{2b}$$

As the quantity of tholins produced is too small for classical elemental analyses, we therefore use HRMS to reach an approximate value of the elemental composition of the tholins. This approach has already been used for various complex extraterrestrial organic matter (Bonnet et al. 2013; Danger et al. 2016; Moran et al. 2020). Hockaday et al. (2009) have shown that intensities weighted average ratios inferred from HRMS data show good agreement (within 15%) with the bulk elemental analysis derived by classical methods. The weighted average elemental composition of the sample is obtained by weighting the element stoichiometry, x, of each species $C_cH_hN_nO_oS_s$ by its corresponding spectral intensity, I, and averaging across all molecular formulas:

$$X_{IWA} = \frac{\sum_i I \times x}{\sum_i I \times (c + h + n + o + s)}. \tag{3}$$

With this approach we assume that intensities are proportional to molecular concentrations, but we must keep in mind that intensity differences between ions can also be due to different ionization yields in the ESI source or different transmission efficiencies that depend on instrumental parameters. To check this impact, the average elemental composition without intensity weighting is also calculated:

$$X_A = \frac{\sum_i x}{\sum_i (c + h + n + o + s)} \tag{4}$$

3. Results

3.1. Peak Assignment

Negative- and positive-ion Orbitrap mass spectra are shown in Figures 2. and 3(a), respectively. Ions generated in negative and positive ionization mode fall within the range $50 < m/z < 450$ and $50 < m/z < 300$, respectively. On a coarse level, the mass spectra of tholins produced from the gas mixture containing H_2S show similar features as the mass spectra of tholins produced from other CO_2-rich gas mixtures, but without H_2S. Indeed, spectra in Figures 1(b) and 7 in Moran et al. (2020) all show a large number of ions over the mass range *m/z* = 150–450, without the obvious regular

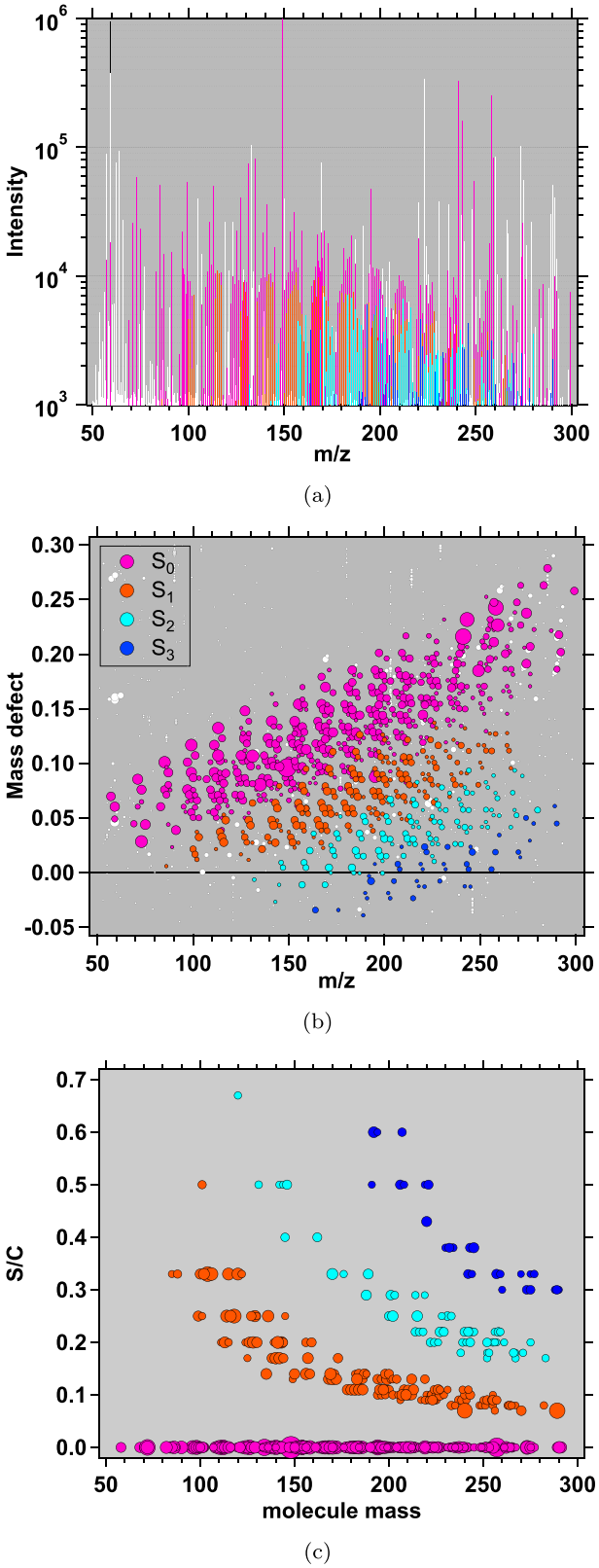

Figure 3. (a) Mass spectrum from $m/z = 50$ to 300 of tholins ($10^4\times$ metallicity, 800 K) in positive ionization mode. Classical representation of the intensity versus mass-to-charge ratio (m/z), in logarithmic scale. (b) Mass defect versus m/z. (c) Variation of S/C ratios as a function of molecule mass for all molecules detected. White represents the original data set while pink, orange, cyan, and blue show the signals attributed to S_0, S_1, S_2, and S_3 classes, respectively. The bubble size scales with mass spectrometric intensity.

Table 1
List of Detected Sulfuric Acid Derivatives

m/z (exp)	Intensity (AU)	Molecular Ion Formula	Error (ppm)
64.970	3.09×10^3	HSO_2^-	0.62
80.965	9.42×10^3	HSO_3^-	−0.49
94.981	1.18×10^5	$CH_3SO_3^-$	−3.15
94.992	5.02×10^2	$N_2H_3SO_2^-$	−3.61
95.976	1.69×10^6	$NH_2SO_3^-$	−1.93
96.960	1.31×10^7	HSO_4^-	−0.68
109.000	1.92×10^3	$C_2H_5SO_3^-$	−1.98
109.990	1.23×10^3	$CNH_4SO_3^-$	−2.31
110.980	1.33×10^6	$CH_3SO_4^-$	0.64
124.990	4.14×10^2	$C_2H_5SO_4^-$	−0.11
140.000	7.68×10^3	$C_2NH_6SO_4^-$	−1.95
140.990	2.86×10^2	$C_2H_5SO_5^-$	−0.77
193.940	2.18×10^3	$NH_4S_2O_7^-$	−1.96
194.930	1.49×10^6	$H_3S_2O_8^-$	4.06

patterns that are apparent in tholins produced from H_2O-rich gas mixtures. Nevertheless, the very low to negative mass defects observed in Figure 3(b) unambiguously reveal the incorporation of sulfur in the molecular compounds (see Figures 6 and 7 in Danger et al. (2013) for MDvM of pure CHON organic matter).

Once calibrated with alkylation series, we obtain 2771 and 828 assigned molecular formulas (AMF) of the form $C_{[0-20]}H_{[1-38]}N_{[0-7]}O_{[0-9]}S_{[0-9]}$, in negative and positive ionization mode, respectively. One hundred and ninety-eight molecular species are generated in both negative and positive ionization mode. Fifty percent of all formulas have an error of ±0.5 ppm, 80% of all formulas have an error of ±1.0 ppm and 100% of formula assignments are within ±4.0 ppm.

The difference between positive and negative ESI modes in a complex mixture is well known (Hertkorn et al. 2008). Depending on the chemical functions carried by molecules, their ionization yield can vary strongly between positive and negative modes, leading to different sets of molecules observed in either ESI mode. Our results show that molecules of the tholins are more efficiently ionized in the negative ESI mode. This suggests that a large fraction of the molecular edifices present in these tholins carry chemical functions presenting proton donor properties, such as carboxylic and sulfonic acid functions; these chemical functions being more easily ionized with negative ESI than with positive ESI. The presence of some molecular species in both modes may be the signature of zwitterionic-like structures easily releasing or capturing a proton. Nevertheless, the considerable extent of noncongruence of positive and negative ions indicates the occurrence of a sizable proportion of tholin molecules that apparently do not contain functional groups which would be easily ionized in both the positive and negative ionization modes under the conditions applied.

3.2. Sulfuric Acid Derivatives

HRMS unambiguously reveals the detection of sulfuric acid (H_2SO_4) as the most intense peak in the negative mode, as displayed in Figure 2(a). Formulas of 14 sulfuric acid derivatives, representing 46% of the total intensity in the negative mode can be identified (Figure 2(a) and Table 1). The most intense peaks include the sulfuric acid dimer $H_4S_2O_8$ and

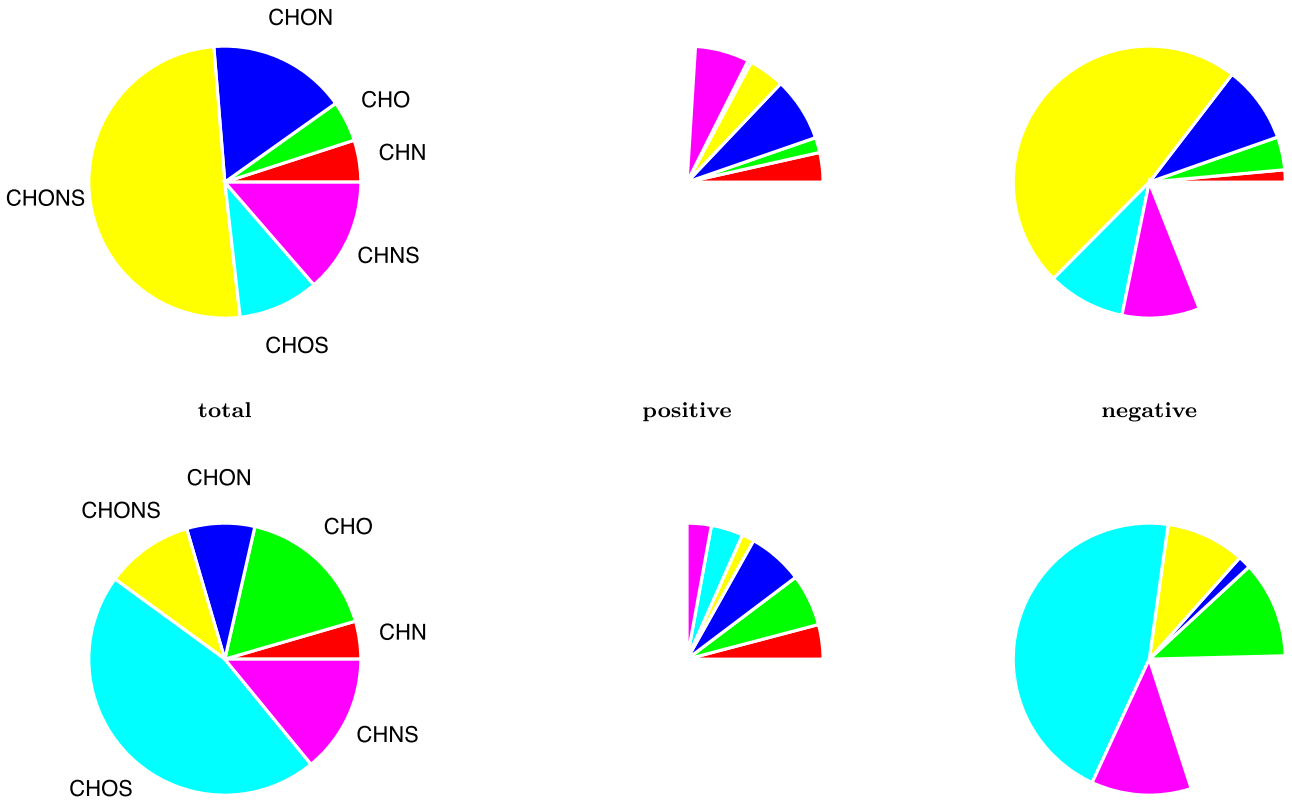

Figure 4. Distribution in molecular groups (CHO/CHN/CHON/CHOS/CHNS/CHONS) of the 3391 organic compounds (Table 2) identified by very high-resolution mass spectrometry. Top: number of AMF in each molecular group; bottom: sum of the peak intensity of the AMF in each molecular group. The sum of the positive and negative ionization modes is more than 100% because some molecules are detected in both modes.

Table 2
Distribution of the Assigned Molecular Formulae and Related Peak Intensity

Ionization mode	CHN	CHO	CHON	CHONS	CHOS	CHS	CHNS	**Total**
Assigned Molecular Formulae								
Positive	121	62	262	147	14	1	221	828
Negative	49	134	312	1628	313	8	313	2757
Both	1	32	17	67	4	0	73	194
Total	169	164	557	1708	323	9	461	3391
Peak Intensity (a.u.)								
Positive	933	1410	1500	338	862	42.2	655	5740
Negative	91.3	2610	347	2130	10300	8.99	2700	18200
Both	1.09	184	17.1	113	753	0	175	1240
Total	1020	3830	1830	2360	10400	51.2	3180	22700

Note. Counts of organosulfur compounds and corresponding intensity for positive, negative ionization mode, and the integral of both modes. "Both" refers to the subsetof molecules that are present in both positive and negative ionization mode.

CH_4SO_4. Sulfuric acid derivatives significantly more intense than the average distribution could reflect a higher ionization yield, rather than a high molecular abundance of mineral sulfur in the sample.

3.3. Organosulfur Compounds

Figure 3(b) shows the presence of complete homologous organosulfur (a general term for species containing C and S) series. These sulfur-containing molecules indicate sulfur is also incorporated into the solid haze and not only in the gas phase (He et al. 2020a). The AMF are organized into the following six molecular groups based on elemental composition (Table 2 and Figure 4): compounds containing only C, H, and O (CHO); compounds containing only C, H, and N (CHN); compounds containing C, H, N, and O (CHON); compounds containing C, H, O, and S (CHOS); compounds containing C, H, N, and S (CHNS); and compounds containing C, H, O, N, and S (CHONS).

The majority of AMF (74%) are sulfur-bearing with the CHONS molecular groups representing 50% of the total number of AMF followed by CHNS, 14%, and CHOS, 10%. Non sulfur-bearing compounds are dominated by CHON, 16%, followed by the CHN and CHO molecular group at 5% each. When taking the peak intensity into account, the order of molecular groups

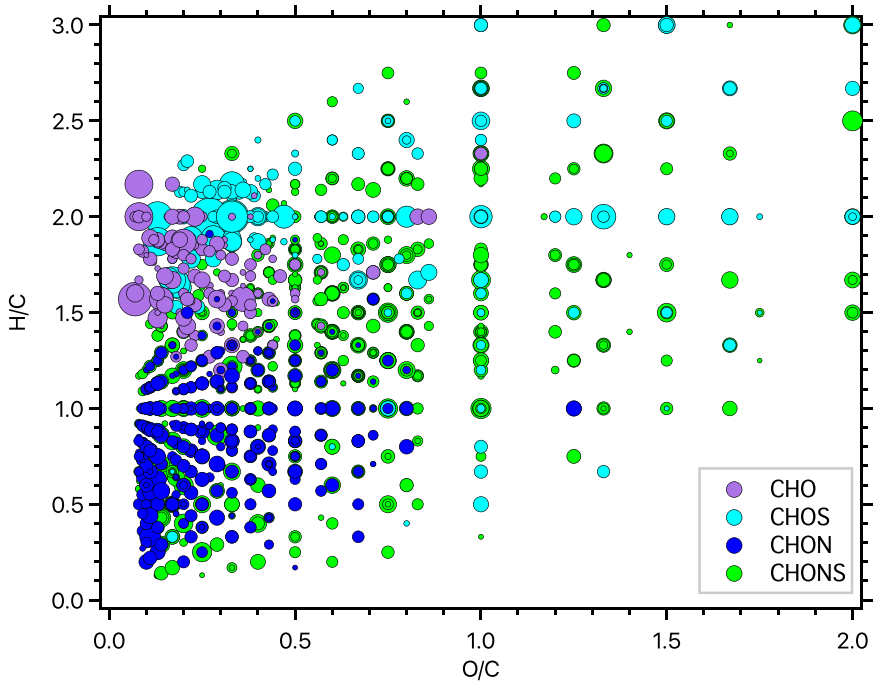

Figure 5. Van Krevelen diagram (H/C vs. O/C) of AMF obtained in negative ionization mode. The color code represents the different molecular groups. The symbol size is proportional to the MS peak intensity.

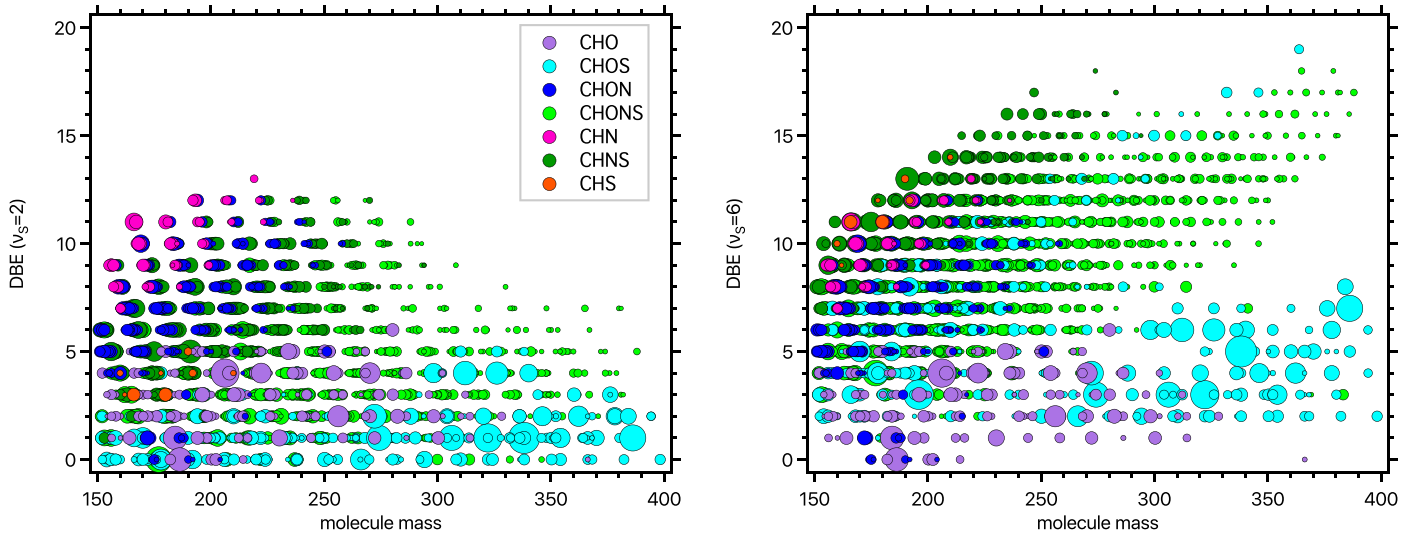

Figure 6. Double Bond Equivalent as a function of the molecule mass assuming that the valence of sulfur is (a) 2 or (b) 6. The color code represents the different molecular groups. The symbol size is proportional to the MS peak intensity.

changes dramatically, 46% of the total intensity being carried by the CHOS molecular group followed by CHNS, 14% and CHONS, 10%. The non sulfur-bearing molecular groups only represent 30% of the total intensity, with CHO, 17%, CHON, 8% and CHN, 5%. Consequently, the molecular diversity observed in such tholins comes mainly from the CHONS group, despite the higher intensity of CHOS species.

Van Krevelen diagrams display the data distribution in two dimensions by taking into account H/C and O/C ratios of each molecular ion and provide an insight into the composition of the analyzed mixture (Hertkorn et al. 2008; Wu et al. 2004). The Van Krevelen representation of the AMF obtained in negative ionization mode is displayed in Figure 5. The CHO and CHON molecular groups both have low O/C ratios with $0.07 < O/C < 1.0$. However, they exhibit very different H/C ratios; that of CHO ($0.9 < H/C < 2.3$) is significantly shifted toward larger values than that of CHON ($0.2 < H/C < 1.9$). These are roughly the same ranges of H/C and O/C as found for molecules originating from CO_2-rich H_2S-free gas mixtures (Figure 8 in Moran et al. 2020). The presence of sulfur in the molecular backbone (CHOS and CHONS molecular groups) leads to a shift of the maximum O/C and H/C to much higher values, up to 2 and 3, respectively.

When considering formulas of organic molecules, qualitatively useful information about the unsaturated character can be readily obtained thanks to the Double Bond Equivalent (DBE) parameter

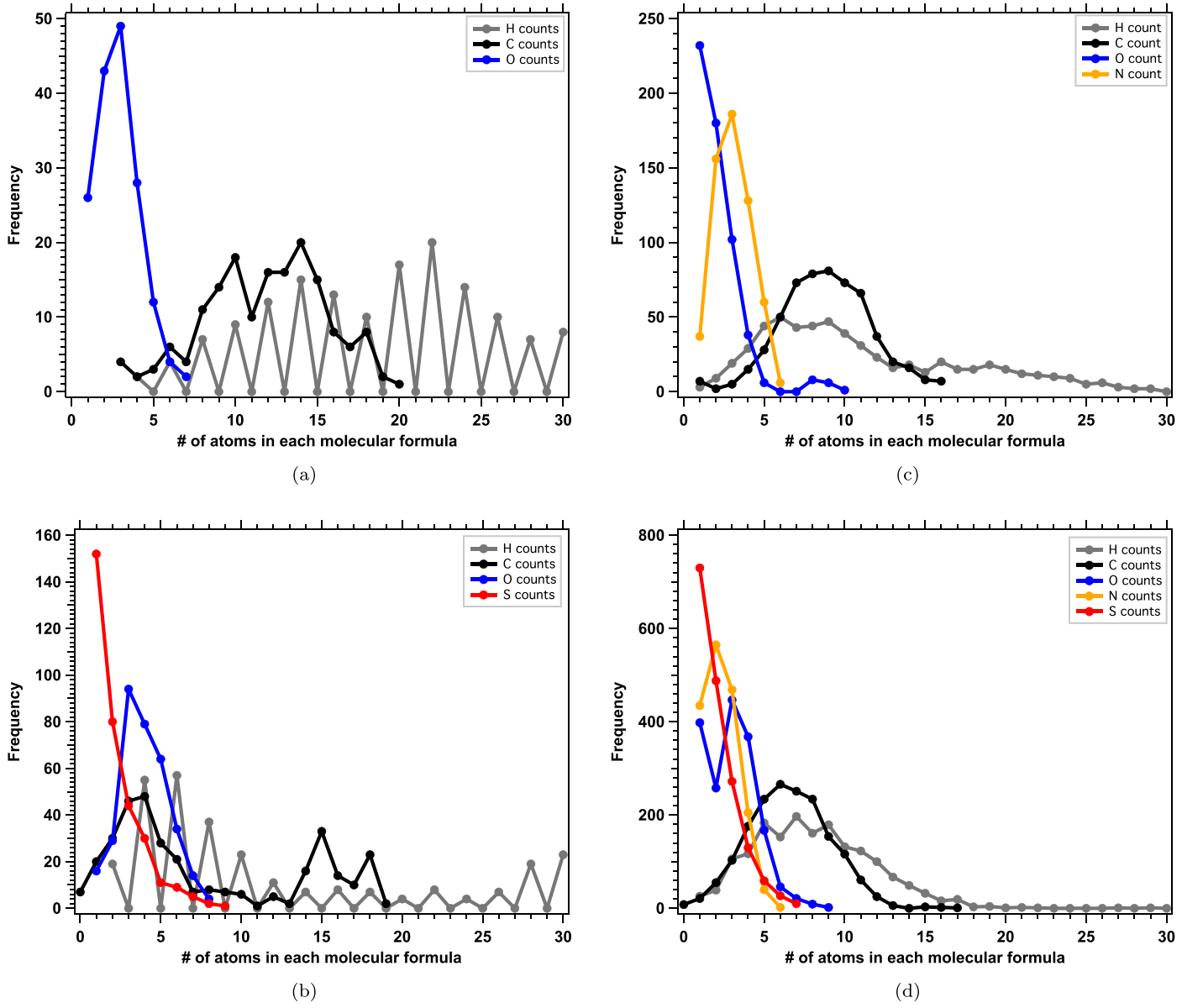

Figure 7. Frequency of occurrence of each number of atoms in AMF within the (a) CHO, (b) CHOS, (c) CHON and (d) CHONS molecular groups. The incorporation of sulfur in the CHO and CHON molecular groups (panels (a) to (b) and (c) to (d)) is associated with an overall increase of the number of oxygen atoms and a decrease of the number of carbon atoms. In the CHO and CHOS molecular groups, the nitrogen rule explains the nonoccurrence of molecules containing an odd number of hydrogen atoms.

(see Equation 2(a)). Figure 6 displays the repartition of DBE for each molecular group, assuming that the valence of sulfur is 2 or 6. The difference between both Figures is an upward shift in DBE of twice the number of sulfur atoms present in each molecular formula. Sulfur in CHS and CHNS molecular groups is mostly expected to exhibit a valence of 2 while in O-bearing groups (CHOS and CHONS), it may exhibit higher valences through formation of one or two double bonds with oxygen.

The CHO and CHS molecular groups exhibit a mostly constant DBE < 6 over the entire mass range, suggesting that most of the molecules belonging to these series have aliphatic structures. In N-bearing groups (CHN, CHNO, CHNS), the degree of unsaturation is higher (DBE $= 4$–12) and it increases with increasing molecular weight in a regular fashion, as observed for Titan tholins (Sarker et al. 2003). This suggests that nitrogen is the dominant carrier of unsaturation, in the form of nitriles or aromatic structures including nitrogen atoms. The increase in DBE of the CHOS and CHONS groups when assuming $\nu_S = 6$ is consistent with the formation of double bonds with oxygen.

Sulfur can readily react with hydrocarbons to make organosulfur (Hickson et al. 2014). Like oxygen, sulfur can formally be inserted into any C-C and C-H bonds; however additional variance exists because of accessible sulfur oxidation states in the range of -2 to $+6$. Figure 7 shows the distribution of atoms in molecular formulas for the four different organosulfur molecular groups. The horizontal displacement of the O and S distribution in CHOS against CHO and CHNOS against CHNO shows the increase in oxygen atoms along with the integration of sulfur. This is remarkable and could imply subsequent addition of sulfur functionalities onto CHO and CHON precursor molecules. As hypothesized for the Murchison meteorite (Schmitt-Kopplin et al. 2010), sulfurization as a single formal insertion of OSO_2 into C-H bonds of CHO and

Table 3
List of Detected Amino Acid Derivatives with Intensity Higher than 10^3

m/z (exp)	Intensity (au)	Molecular Ion Formula	Error (ppm)	Possible Metabolite
110.829	1.11×10^4	$C_3H_5O_3S^+$	0.50	Mercaptopyruvate
123.011	1.33×10^3	$C_3H_7O_3S^+$	0.80	3-Mercaptolactate
150.971	1.49×10^3	$C_3H_3O_5S^-$	−0.20	3-Sulfinylpyruvate
151.984	1.03×10^3	$C_3H_6NO_2S2^-$	0.33	Thiocysteine
152.002	1.26×10^4	$C_3H_6NO_4S^-$	0.72	3-Sulfino-L-alanine/L-cysteine sulfinate
164.039	1.84×10^3	$C_5H_{10}NO_3S^-$	0.02	L-Methionine S-oxide
169.008	3.77×10^3	$C_6H_5N_2O_2S^-$	−0.28	Thiourocanic acid
177.034	2.11×10^3	$C_5H_9N_2O_3S^-$	0.03	Cys-Gly
179.038	1.93×10^3	$C_6H_{11}O_4S^-$	0.27	5-Methylthio-D-ribose
191.050	1.21×10^3	$C_6H_{11}N_2O_3S^-$	0.11	Ala-Cys
196.011	1.46×10^3	$C_5H_{10}NO_3S2^-$	−0.00	CysteineMercaptoethanol disulfide
207.045	1.98×10^3	$C_6H_{11}N_2O_4S^-$	0.39	Cys-Ser
221.060	1.23×10^3	$C_7H_{13}N_2O_4S^-$	0.01	L-Cystathionine/Thr-Cys

Table 4
Average and Intensity Weighted Average Elemental Ratios (wt%) for Positive and Negative Ionization Mode, and the Integral of Both Modes

Elements	Initial Gas	Tholins					
		Average			Intensity Weighted Average		
		Positive	Negative	**Total**	Positive	Negative	**Total**
H	0.9	7.2	3.9	4.5	8.8	6.2	6.4
C	26.5	54.8	38.5	41.3	63.6	36.2	39.1
N	9.7	18.2	13.2	14.2	10.9	2.4	3.6
O	61.2	7.3	18.9	17.0	9.4	32.4	30.0
S	1.6	12.5	25.4	23.0	7.2	22.8	20.9

CHNO compounds would address the occurrence of oxidized sulfur in the tholins.

3.4. Prebiotic Compounds

A variety of formulas corresponding to amino acids, nucleotide bases, and sugar derivatives have been detected before by HRMS in tholins of Titan and exoplanets (Hörst et al. 2012; Moran et al. 2020). We searched in our list of stoichiometric formulas for those that could correspond to amino acid metabolites and peptides of proteinogenic amino acids according to a comprehensive metabolite database, containing 41,623 potential metabolites (Creek et al. 2011). We obtain 11 matches with amino acid metabolism and four with dipeptides (Table 3). However, because of the weak molecular ion intensities, the actual structure of the molecules cannot be confirmed with MS/HRMS or high-performance liquid chromatography (HPLC), which prevents us from determining which isomer(s) are present in the samples and therefore confirming the attribution to any amino acid derivatives.

3.5. Elemental Composition

The elemental composition of the soluble fraction of the tholins is obtained by averaging elemental ratios obtained in negative and positive ionization mode, with or without intensity weighing (see Equations (3) and (4)). Elemental ratios are presented in Table 4. Both average and intensity weighted average elemental ratios are higher in the positive mode for nitrogen and in the negative mode for oxygen and sulfur. This effect can be explained by the different ionization efficiency of specific chemical functions in the ESI process. Acidic molecular species, e.g., compounds with carboxylic acid or sulfonic acid groups, are preferentially deprotonated, while basic species, e.g., amines or amides, are preferentially protonated.

In the negative mode, the average and intensity weighted average of O elemental ratios are very different. This is consistent with molecules containing an excess of oxygen, such as sulfuric acid derivatives, being present with high intensities. The CHOS group is emblematic of such behavior, with a low number of AMF (10%), while representing 66% of the total intensity (Figure 4). The opposite effect is observed for nitrogen in both positive and negative mode, revealing a depletion of nitrogen, correlated with the CHONS group, which represents a high number of attributions (50%) but only 10% of the total intensity (Figure 4). This effect can be explained by either a different overall abundance of the corresponding molecules or a different ionization efficiency of specific chemical functions, e.g., in negative mode, carboxylic acids have a better ionization yield than alcohol, aldehyde, or keto functions and amines have a better ionization efficiency than nitriles or imines. Considering the different DBE ranges covered by the different groups (Figure 6), one can expect that the chemical functions are not similar in all groups. The total elemental ratios are heavily biased toward the negative mode because of the higher number of AMF compared with the positive mode. Again, the total intensity weighted average values indicate a depletion in nitrogen and an increase in oxygen compared with average values.

Dividing the mass of the initial gas mixture (66.96 g) by the total mass of the tholins (78.5 mg) gives a 0.117% yield. From the amount of decomposed H_2S, the mass fraction of sulfur in the tholins is calculated to be 3.6% (He et al. 2020a). The

Orbitrap measurements suggest that the soluble fraction is made of about 22% of S by mass. This difference may first seem surprising, but it actually makes sense because sulfur-containing organic compounds are polar and should be soluble in polar solvents such as CH_3OH/CH_2Cl_2. Unlike for pure CHON tholins, it is therefore not unexpected that the insoluble part contains no or very little sulfur and that the soluble fraction is not representative of the bulk.

While sulfur is very deficient in the gas (1.6%), its abundance is increased by a factor of ∼14 in the soluble fraction of the tholins. Carbon, as the major backbone of the molecules, is increased by about 50%. Nitrogen and oxygen are depleted by a factor of 2–3. The efficient incorporation of sulfur and the observation that including H_2S in the initial gas mixture produces more solid particles than without H_2S (He et al. 2020a) is indicative of the increased reactivity of sulfur toward its addition to carbon, compared with nitrogen and oxygen.

Previous analogues representative of CO_2-rich/H_2S-free exoplanet atmospheres were composed of ∼60% C, ∼8% H, ∼19% O and an uncertain amount of N (Table 2 in Moran et al. 2020). Therefore, the competition for inclusion of S in the tholins does happen at the expense of C, which is in agreement with the shift of the distribution of the number of C in molecular formulas toward lower values from CHO to CHOS and from CHON to CHONS (Figure 7). These observations support the existence of sulfur-bearing functional groups with oxygen, such as OSO_2 but not OCS, despite its identification in the gas phase (He et al. 2020a).

4. Astrophysical Discussion

While our exoplanet aerosol analogue shares some physical characteristics with previous analogues representative of CO_2-rich/H_2S-free exoplanet atmospheres (He et al. 2018b, 2020a), mass spectrometry shows they are chemically distinct (Moran et al. 2020 and this work) and that a diverse, rich, and active sulfur chemistry is taking place. In the context of the early Earth, Farquhar et al. (2001) saw H_2SO_4 in the aerosol formed after low-wavelength photolysis of $SO_2/CO_2/H_2O$, a conclusion also shared by DeWitt et al. (2010) after exposure of a $SO_2/CO_2/H_2/N_2$ gas mixture to an electrical discharge. Some amount of low-mass organosulfates, such as methyl sulfonic acid (CH_3SO_3H), was observed in the aerosols of DeWitt et al. (2010). Formation of elemental sulfur (S_8) was also found in these experiments, and was actually the dominant S aerosol in more reducive conditions. Here, with a similar gas mixture but where SO_2 has been replaced by H_2S, we report the formation of H_2SO_4 and some derivatives as well as thousands of organosulfur compounds. As the boiling point of S_8 is 717 K, it should stay in the gas phase in our experiment (800 K), but was not detected there (He et al. 2020a). The formation of organosulfur compounds from the ultraviolet photochemistry of trace amounts of H_2S in CH_4/N_2 mixtures has recently been presented (Reed et al. 2020). Our results support the coupling between carbon and sulfur chemistries, whatever the oxidation state of carbon is (CO_2/CO versus CH_4).

A hypothetical warm (800 K) exoplanet around a given host M star (3000 K) would have an energy density of ∼14 W m^{-2} in the range of 1 to 300 nm, which is important for atmospheric photochemistry. Therefore, a 72-hour exposure to the AC glow discharge in our experiment (with an estimated energy density of 170 W m^{-2}) roughly corresponds to 51 days of UV irradiation from the host M star. Sulfur photochemistry models have been developed for a wide range of exoplanets' temperature and metallicity to infer the impact of light gas-phase sulfur-bearing compounds on the chemistry and temperature. According to these models, sulfur chemistry tends to build toward sulfuric acid and the relatively photolytically stable S_8 molecule. Sulfur photochemistry must begin with photolysis of H_2S, or its chemical attack by H and OH, released from photolysis of H_2 and H_2O. S can then be successively oxidized by OH to SO, SO_2, and SO_3 or H_2SO_4. On the other hand, HS and S_2 are two highly reactive species that can be generated chemically from H_2S, initiating the polymerization of sulfur up to S_8 (Hu et al. 2013; Zahnle et al. 2009, 2016).

It has been shown that sulfur aerosols drastically alter a planet's geometric albedo, but the exoplanet atmospheric chemistry models that these results are based upon only consider condensation of S_8 and H_2SO_4 (Gao et al. 2017; Hu et al. 2013). Neubauer et al. (2012) computed that H_2SO_4-clouds affect the surface temperatures, which has some impact on the position of the life supporting zone. Our experimental simulations show that organosulfur species are likely an important component of the haze in exoplanet atmospheres and should be taken into account in these models. Hazes can also act as condensation nuclei, and a large fraction of sulfur in the aerosols may have an impact on cloud formation. We have shown that the color of tholin films varies significantly as a function of metallicity and temperature (He et al. 2018b). Here, the tholin particles were sort of grayish, not dark gold as in standard Titan experiments, suggesting that the optical constants derived from Titan analogues (e.g., Khare et al. 1984) are not relevant. The haze optical properties affect the reflectance spectrum and how much radiation can reach the surface (Arney et al. 2016). Indeed, the radiation that reaches the surface under a Titan-like haze has a higher proportion of longer, redder wavelengths compared with shorter, bluer wavelengths, which would not be the case with a more grayish haze. Further work is required to determine the optical properties of exoplanet haze analogues and quantify their impact in future models.

The presence of H_2SO_4 and organosulfur compounds within high-metallicity atmospheres might influence our view on the search of habitability and biosignatures. The integration of sulfur in aerosols may serve as an irreversible sink for gas-phase sulfur, as the sedimentation of aerosols at the surface would lead to a chemically stable solid reservoir. There are multiple ways that life can produce H_2S and other biogenic organosulfur gases (e.g., CS_2, OCS, CH_3SH, CH_3SCH_3), including the reduction of sulfate and the disproportionation of sulfur compounds of intermediate oxidation states. Modeling studies have shown that organosulfur gases can provide additional hydrocarbon sources, enhancing haze formation through photochemistry. Therefore, detection of haze at low CH_4/CO_2 ratios could suggest the presence of these biogenic sulfur gases and imply biological activity on an exoplanet (Arney et al. 2018). Our results show that the inclusion of direct sulfur-carbon chemistry in these models may increase haze formation even more. Although H_2S is expected to be short lived in terrestrial exoplanet atmospheres, making direct detection difficult (Hu et al. 2013), it is more chemically favored in a broad range of sub-Neptune type atmospheres (Moses et al. 2013). In the near term, the James Webb Space Telescope will be able to probe the broad range of H_2S features throughout the infrared via transmission and emission

observations of exoplanets. Future observing facilities that can probe the light reflected from exoplanet atmospheres may allow better inference of the presence of H_2S through aerosol-related features, especially for terrestrial planets.

5. Conclusions

In this paper, we have shown experimentally that an active and diverse sulfur chemistry can be triggered by high-energy irradiation of H_2S in a CO_2-rich gas mixture. Sulfuric acid, as well as thousands of organosulfur compounds, are incorporated into haze analogues. The soluble fraction of the particles is heavily enriched in sulfur, suggesting that aerosol formation may be an irreversible sulfur sink in warm exoplanet atmospheres. Models have shown that gas-phase sulfur-bearing compounds as well as S_8 and H_2SO_4 condensation clouds alter the planet's atmospheric chemistry, temperature, and geometric albedo. An important caveat of these models is that organosulfur aerosols were not taken into account. Our results indicate that they would likely impact the sulfur budget and optical properties of the aerosols and their consideration in future models should be considered.

This work is supported by the French National Research Agency in the framework of the "Investissements d'Avenir" program (ANR-15-IDEX-02), through the funding of the Origin of Life project of the Université Grenoble Alpes, the French Space Agency (CNES) under their "Exobiologie, Exoplanètes et Protection Planétaire" program and NASA Astrophysics Research and Analysis Program NNX17AI87G. Cédric Wolters acknowledges a PhD fellowship from CNES/ANR (ANR-16-CE29-0015 2016-2021). S. E. Moran acknowledges support from NASA Earth and Space Science Fellowship grant 80NSSC18K1109.

ORCID iDs

Véronique Vuitton https://orcid.org/0000-0001-7273-1898
Sarah E. Moran https://orcid.org/0000-0002-6721-3284
Chao He https://orcid.org/0000-0002-6694-0965
Cédric Wolters https://orcid.org/0000-0002-9710-4740
Julianne I. Moses https://orcid.org/0000-0002-8837-0035
Nikole K. Lewis https://orcid.org/0000-0002-8507-1304
Sarah M. Hörst https://orcid.org/0000-0003-4596-0702

References

Arney, G., Domagal-Goldman, S. D., & Meadows, V. S. 2018, AsBio, 18, 311
Arney, G., Domagal-Goldman, S. D., Meadows, V. S., et al. 2016, AsBio, 16, 873
Arney, G. N., Meadows, V. S., Domagal-Goldman, S. D., et al. 2017, ApJ, 836, 49
Benneke, B., Knutson, H. A., Lothringer, J., et al. 2019, NatAs, 3, 813
Bonnet, J.-Y., Thissen, R., Frisari, M., et al. 2013, IJMSp, 354, 193
Cable, M., Hörst, S., Hodyss, R., et al. 2012, Chem. Rev., 112, 1882
Creek, D. J., Jankevics, A., Breitling, R., et al. 2011, AnaCh, 83, 8703
Danger, G., Fresneau, A., Abou Mrad, N., et al. 2016, GeCoA, 189, 184
Danger, G., Orthous-Daunay, F.-R., de Marcellus, P., et al. 2013, GeCoA, 118, 184
DeWitt, H., Hasenkopf, C. A., Trainer, M. G., et al. 2010, AsBio, 10, 773
DeWitt, H.-L., Trainer, M.-G., Pavlov, A.-A., et al. 2009, AsBio, 9, 447
Farquhar, J., Savarino, J., Airieau, S., & Thiemens, M. 2001, JGR, 106, 32829
Fresneau, A., Mrad, N. A., LS d'Hendecourt, L., et al. 2017, ApJ, 837, 168
Gao, P., Fan, S., Wong, M. L., et al. 2017, Icar, 287, 116
Gautier, T., Danger, G., Mousis, O., et al. 2020, E&PSL, 531, 116011
He, C., Hörst, S. M., Lewis, N. K., et al. 2018a, AJ, 156, 38
He, C., Hörst, S. M., Lewis, N. K., et al. 2018b, ApJL, 856, L3
He, C., Hörst, S. M., Lewis, N. K., et al. 2019, ECS, 3, 39
He, C., Hörst, S. M., Lewis, N. K., et al. 2020a, NatAs, 4, 986
He, C., Hörst, S. M., Lewis, N. K., et al. 2020b, PSJ, 1, 51
Hertkorn, N., Frommberger, M., Witt, M., et al. 2008, Anal. Chem., 80, 8908
Hickson, K., Loison, J., Cavalié, T., Hébrard, E., & Dobrijevic, M. 2014, A&A, 572, A58
Hockaday, W. C., Purcell, J. M., Marshall, A. G., Baldock, J. A., & Hatcher, P. G. 2009, Limnol. Oceanogr.: Methods, 7, 81
Hörst, S., Yelle, R., Buch, A., et al. 2012, AsBio, 12, 809
Hörst, S. M., He, C., Lewis, N. K., et al. 2018, NatAs, 2, 303
Hu, R., Seager, S., & Bains, W. 2013, ApJ, 769, #6
Jovanović, L., Gautier, T., Vuitton, V., et al. 2020, Icar, 346, 113774
Khare, B., Sagan, C., Arakawa, E., et al. 1984, Icar, 60, 127
Kreidberg, L., Bean, J. L., Désert, J.-M., et al. 2014, Natur, 505, 69
Libby-Roberts, J. E., Berta-Thompson, Z. K., Désert, J.-M., et al. 2020, AJ, 159, 57
Lothringer, J. D., Benneke, B., Crossfield, I. J. M., et al. 2018, AJ, 155, 66
Maillard, J., Carrasco, N., Schmitz-Afonso, I., Gautier, T., & Afonso, C. 2018, E&PSL, 495, 185
Marley, M. S., Ackerman, A. S., Cuzzi, J. N., & Kitzmann, D. 2013, Comparative Climatology of Terrestrial Planets (Tucson: University of Arizona Press), 367
Moran, S. E., Hörst, S. M., Vuitton, V., et al. 2020, PSJ, 1, 17
Moses, J. I., Line, M. R., Visscher, C., et al. 2013, ApJ, 777, 34
Neubauer, D., Vrtala, A., Leitner, J. J., Firneis, M. G., & Hitzenberger, R. 2012, P&SS, 73, 397
Orthous-Daunay, F.-R., Piani, L., Flandinet, L., et al. 2019, GeocJ, 53, 21
Orthous-Daunay, F.-R., Thissen, R., & Vuitton, V. 2020, in IAU Conf. Proc. 350, Laboratory Astrophysics: From Observations to Interpretation, ed. F. Salama & H. Linnartz (Cambridge: Cambridge Univ. Press), 193
Reed, N. W., Browne, E. C., & Tolbert, M. A. 2020, ECS, 4, 897
Sarker, N., Somogyi, Á., Lunine, J., & Smith, M. 2003, AsBio, 3, 719
Schmitt-Kopplin, P., Gabelica, Z., Gougeon, R., et al. 2010, PNAS, 107, 2763
Somogyi, Á, Thissen, R., Orthous-Daunay, F.-R., & Vuitton, V. 2016, International Journal of Molecular Sciences, 17, 439
Titov, D. V., Ignatiev, N. I., McGouldrick, K., Wilquet, V., & Wilson, C. F. 2018, SSRv, 214, 126
Vuitton, V., Bonnet, J.-Y., Frisari, M., et al. 2010, FaDi, 147, 495
Wolters, C., Flandinet, L., He, C., et al. 2020, RCMS, 34, e8818
Wu, Z., Rodgers, R. P., & Marshall, A. G. 2004, Anal. Chem., 76, 2511
Zahnle, K., Marley, M. S., Freedman, R. S., Lodders, K., & Fortney, J. J. 2009, ApJL, 701, L20
Zahnle, K., Marley, M. S., Morley, C. V., & Moses, J. I. 2016, ApJ, 824, 137